Journal of Materials Chemistry C

Accepted Manuscript

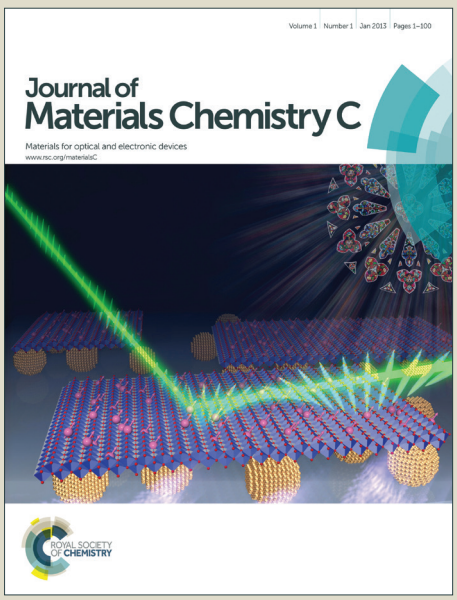

ROYAL SOCIETY OF CHEMISTRY

www.rsc.org/materialsC

Journal of Materials Chemistry

PAPER

$Ba_4AgGa_5Pn_8$ (Pn = P, As): New Pnictide-Based compounds with Nonlinear Optical Potential

Cite this: DOI: 10.1039/x0xx00000x

Ming-yan Pan,[a] Zu-ju Ma,[b] Xiao-cun Liu,[a] Sheng-qing Xia, *[a] Xu-tang Tao [a] and Ke-chen, Wu *[b]

Received,
Accepted

DOI: 10.1039/x0xx00000x

www.rsc.org/materials

Two new quaternary pnictide-based multinary compounds, $Ba_4AgGa_5P_8$ and $Ba_4AgGa_5As_8$, were synthesized from the Pb-flux reactions. By using the single crystal X-ray diffraction technique the structures are determined to crystallize in a new type with the noncentrosymmetric (NCS) space group *Iba2* (No. 45) (cell parameters: a = 7.294(9)/7.4769(8) Å, b = 18.03(2)/18.5766(19) Å, c = 6.557(8)/6.7590(7) Å for the P- and As-containing compounds, respectively. Theoretical calculations indicate strong SHG responses for both compounds, which are approximately two times larger than that of $AgGaSe_2$. Based on the calculated cutoff-energy-depending static SHG coefficients, the large NLO coefficients of these compounds should originate from the distorted $GaPn_4$ tetrahedra, which construct various layers and chains giving rise to a large polarization. Both compounds have moderate birefringence (Δn), 0.157 and 0.206 for $Ba_4AgGa_5P_8$ and $Ba_4AgGa_5As_8$, respectively, suitable for the phase-matching condition in the SHG process.

Introduction

Nonlinear optical (NLO) materials are indispensable for the application on laser frequency conversion. Compared with those materials in ultraviolet/visible/near-infrared region,[1-6] practical NLO crystals for the mid-infrared applications are relatively rare and currently, the most promising candidates are still based on several types of chalcogenide and pnictide semiconductors, such as $AgGaS_2$,[7,8] $AgGaSe_2$,[9,10] $ZnGeP_2$.[11-13] Thus, exploration of new materials with high performance for such applications will be necessary. Aiming at this purpose, there were many chalcogenides synthesized recently which have already showed potential for the mid-infrared utilization.[14-17] The idea of designing these compounds are through the combination of different kinds of metal centers with different preferences on size coordination and packing characteristics, which can be a good routine to construct new noncentrosymmetric (NCS) compounds with large polarity. Such examples have been frequently reported, such as $K_3Ta_2AsS_{11}$,[18] $Ba_{23}Ga_8Sb_2S_{23}$[19]and $Ba_4CuGa_5S_{12}$.[20]

The discovery of new pnictide-based NLO compounds was relatively rare and in this field studies seem still predominantly focused on the classical binary semiconductors like GaAs[21,22] and ternary chalcopyrite semiconductors such as $CdSiP_2$,[23] $CdGeAs_2$.[24] In our previous work, we have discovered a new quaternary arsenide $Ba_{13}Si_6Sn_8As_{22}$[25] crystallizing in noncentrosymmetric structure and featuring adamantane-like $[Si_4As_{10}]$ clusters for which strong polarity can be expected. In this work we extend our studies to phosphides and successfully obtained two quaternary pnictides $Ba_4AgGa_5P_8$ and $Ba_4AgGa_5As_8$. These two compounds are isostructural and both crystallize in the noncentersymmetric (NCS) space group *Iba2* (No. 45). The measured optical band gaps for $Ba_4AgGa_5P_8$ and $Ba_4AgGa_5As_8$ are 1.4 eV and 0.8 eV and according to the theoretical evaluation, these two compounds have large second harmonic generation (SHG) coefficients, which are about two times larger than that of $AgGaSe_2$.

Results and Discussion

Structure Description

$Ba_4AgGa_5P_8$ and $Ba_4AgGa_5As_8$ are isotypic compounds and they both crystallize in the orthorhombic noncentrosymmetric (NCS) space group *Iba2* (No. 45). In each unit cell, there are totally 8 Ba^{2+}, 2 Ag^{+} and 10 Ga^{3+} cations, which are charge-balanced by 16 P^{3-} or As^{3-} anions. As indicated in Figure 1, the structure can be viewed as stack of GaP layers, sandwiched by the $(Ag,Ga)P_2$ chains. In this manner, a three dimensional polyanion framework $[AgGa_5P_8]^{8-}$ is constructed. In each GaP slab, an interesting Ga_3P_3 six-membered ring is formed, similar to the NiSi network of TiNiSi.[26] The $(Ag,Ga)P_2$ polyanion chain is isotypic to the ZnP_2 chain in Ba_2ZnP_2,[27] except for the difference that the Ag and Ga atoms are disordered within the Zn sites in the Ba_2ZnP_2 structure. A detailed view of the GaP plane is shown in Figure 1b, the distorted GaP_4 tetrahedra are related by n-glide plane symmetry {*x+1/2, -y+1/2, z*} or {*-x+1/2, y+1/2 , z*}, which gives rise to a large polarization along the *c*-axis but cancel out the polarization along *a*- or *b*-axis.

ARTICLE

Besides, the $(Ag,Ga)P_2$ chains propagating along the *c*-axis with 2_1-symmetry will also enlarge the polarization (Figure 1c). These crystallographic results indicate that $Ba_4AgGa_5P_8$ and $Ba_4AgGa_5As_8$ may have strong SHG responses originating from the anions framework $(AgGa_5P_8)^{8-}$, which is proved by the cutoff-energy-dependent SHG coefficient calculation below.

Table 1. Selected crystal data and structure refinement parameters for $Ba_4AgGa_5P_8$ and $Ba_4AgGa_5As_8$.

Formula	$Ba_4AgGa_5P_8$	$Ba_4AgGa_5As_8$
Fw / g·mol^{-1}	1253.59	1605.19
T/ K	296(2)	296(2)
Radiation, wavelength	Mo-Kα, 0.71073 Å	
Crystal system	Orthorhombic	
Space group	*Iba2* (No. 45)	
a / Å	7.294(9)	7.4769(8)
b / Å	18.03(2)	18.5766(19)
c / Å	6.557(8)	6.7590(7)
V / Å^3	862.0(18), Z=2	938.79(17), Z=2
ρ_{calc} / g·cm^{-3}	4.830	5.679
GOOF	1.121	1.172
Final R indices [a] [I>2$\sigma_{(I)}$]	R_1 = 0.0450 wR_2 = 0.1177	R_1 = 0.0207 wR_2 = 0.0496
Final R indices [a] [all data]	R_1 = 0.0488 wR_2 = 0.1211	R_1 = 0.0213 wR_2 = 0.0499

[a] $R_1 = \sum||F_o| - |F_c||/\sum|F_o|$; $wR_2 = [\sum[w(F_o^2 - F_c^2)^2]/\sum[w(F_o^2)^2]]^{1/2}$, and w = $1/[\sigma^2F_o^2 + (A\cdot P)^2 + B\cdot P]$, P = (Fo2 + 2Fc2)/3; A and B are weight coefficients.

Since $Ba_4AgGa_5P_8$ and $Ba_4AgGa_5As_8$ have the same structure type, only $Ba_4AgGa_5P_8$ is chosen for detailed structure analysis. As mentioned above, the GaP_4 tetrahedra are very distorted: although the Ga-P bonding distances have very minor differences (2.365(5) ~ 2.380(4)Å), the related ∠PGaP bonding angles fall into a broad range from 95.98(13) to 123.24(19)º, which significantly deviate from the bonding angle of a regular tetrahedron. These values are also comparable to those analogues such as $Ba_6Ga_2P_6$,[28] $EuGa_2P_2$.[29] However, the interatomic distances between the mixed Ag/Ga and P atoms range from 2.529(7) to 2.546(7) Å, obviously longer than the regular Ga-P bonds. Compared with the typical Ag-P covalent bonds in BaAgP (2.596 Å),[30] it is not surprising to observe that these (Ag,Ga)-P bonds are a little shorter. These results strongly suggest the substantial mixing between the Ga and Ag atoms in the center of P_4 tetrahedra. The mixing between the Ag and Ga atoms is further supported by a simple electron counting of the system. As mentioned above, an equal distribution of Ag and Ga at the mixed site will result in the stoichiometric formula $(Ba^{2+})_4Ag^+(Ga^{3+})_5(P^{3-})_8$, which is exactly charge-balanced. This phenomenon implies that the electron requirement still plays a key role in governing the structural formation of these multinary phases, which is supported by the theoretical calculations as well as the related optical absorption properties below.

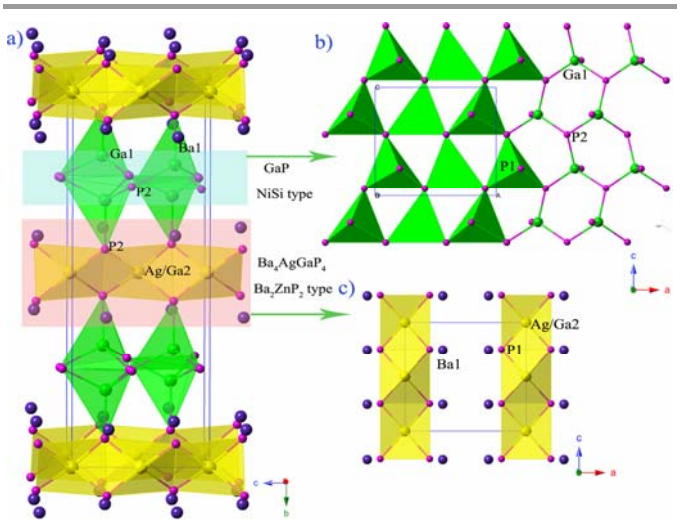

Figure 1. (a) Polyhedral structure view of $Ba_4AgGa_5P_8$, viewed down the a-axis. The Ba, Ga and P atoms are represented by purple, green and pink spheres, respectively. The mixed $(Ag,Ga)P_4$ tetrahedra are plotted in yellow colors. (b) A close-up view of the GaP layer along the b-axis. (c) $(Ag,Ga)P_4$ chain structure with Ag and Ga atoms mixed at the center of P_4 tetrahedra.

Thermal stability

The results of differential thermal analysis (DTA) and thermogravimetry (TG) measurements are presented in Figure S1 (Supporting Information). For $Ba_4AgGa_5P_8$, there is no significant mass loss observed over the whole measured temperature range, and an endothermic peak appearing at around 600 K in the DSC curves should be designated as the melting process of Pb left from the flux. For $Ba_4AgGa_5As_8$, the endothermic peak at around 1200K indicates the decomposition process of the compound, which results in amorphous phases confirmed by the powder XRD patterns.

Optical Absorption Spectrum

The absorption spectra of $Ba_4AgGa_5P_8$ and $Ba_4AgGa_5As_8$ were collected by using the diffusive reflectance technique at room temperature and the data are presented in Figure S3. The measured optical band gaps are 1.4 eV and 0.8 eV for $Ba_4AgGa_5P_8$ and $Ba_4AgGa_5As_8$, respectively. These values are consistent with their black color and follow the theoretical prediction base on the DFT methods. There are also some small peaks appearing in the curves, which probably correspond to the absorption processes of some unknown amorphous impurities and obviously can not be designated through the powder X-ray diffraction patterns (Figure S2).

Electronic structure and Nonlinear Optical Property calculations

The electronic band structures of $Ba_4AgGa_5P_8$ and $Ba_4AgGa_5As_8$ are presented in Figure S4 (Supporting

Information). These compounds both exhibit direct band gaps, which are 1.1 and 0.7 eV for the phosphide- and arsenide-containing compounds, respectively. The experimental observations suggest close results of 1.4 and 0.8 eV, a little larger than the theoretical prediction owing to the well-known underestimation of the band gaps by PBE methods. The calculated Density of States (DOS) for $Ba_4AgGa_5P_8$ and $Ba_4AgGa_5As_8$ are similar due to the same structure type. Thus, here we only choose $Ba_4AgGa_5P_8$ for detailed discussions and the data of $Ba_4AgGa_5As_8$ are provided in Supporting Information (Figure S5). The total and partial DOS for $Ba_4AgGa_5P_8$ are shown in Figure 2. The highest valence band (HVB) is mainly derived from P 3p states, whereas the lowest conduction band (LCB) is a mixture of P 3p, Ga 4p and Ba 5d orbitals. The valence bands (VB) from -7.0 eV to the Fermi level (E_f) are substantially contributed by Ga 4p and P 3p, indicating strong covalent bonds between the Ga and P atoms, which as well will play a very important role in affecting the related optical properties. The states of Ba mainly occupy the region above E_f, implying that the role of Ba is still electron donor and the interactions between cation and anions are probably rather weak.

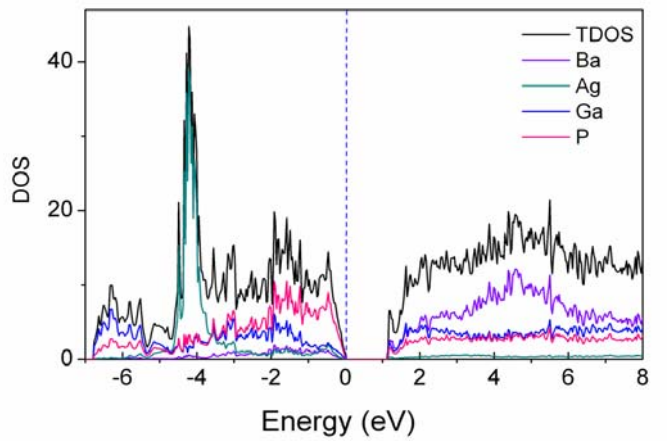

Figure 2. Calculated total DOS and projected DOS for $Ba_4AgGa_5P_8$. The dotted line marked the Femi level.

Subsequent optical property calculations were thus applied with scissor values of 0.24 and 0.1 eV for $Ba_4AgGa_5P_8$ and $Ba_4AgGa_5As_8$. It has been proved to be adequate for predicting the static SHG coefficients of semiconductors using the "sum over states" method by adding scissor operators.[31-33] The corresponding absorption coefficient α and birefringence (Δn) were also calculated. The basic absorption edges (Figure S6) are 1.15 and 0.65 eV for $Ba_4AgGa_5P_8$ and $Ba_4AgGa_5As_8$, comparable with the experimental results. The static birefringence (Δn) (Figure S7) are also moderate, 0.157 and 0.206 for $Ba_4AgGa_5P_8$ and $Ba_4AgGa_5As_8$, respectively. These theoretical results suggest that these two crystals may be suitable for the phase-matching condition in the SHG process.

In order to calculate the nonlinear optical properties, a model with C2 (No. 5) symmetry was built (Figure S10) to solve the disorder between Ag and Ga atoms. Based on the Kleinman symmetry [34] as well as the space group, $Ba_4AgGa_5P_8$ has four nonvanishing independent SHG coefficient tensors (d_{14}, d_{16}, d_{22} and d_{34}). Among them, the value of d_{16} is the smallest, so only d_{14}, d_{22}, d_{34} are shown. As indicated in Figure 3, the frequency-dependent SHG coefficient d_{34} of $Ba_4AgGa_5P_8$ is 77.4pm/V, which is about two times larger than the d_{36} of $AgGaSe_2$.[35]

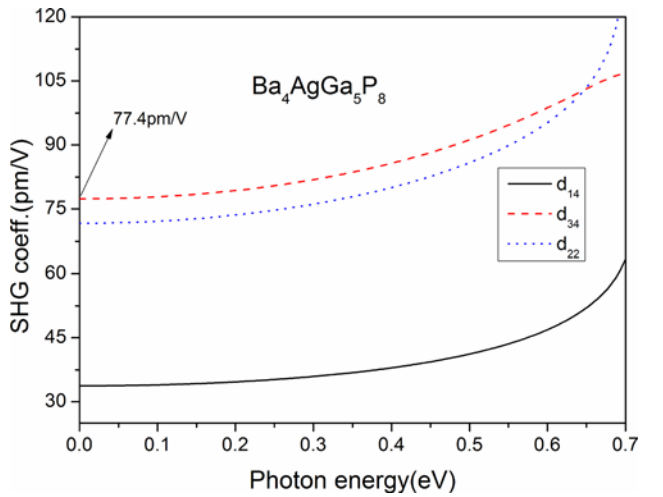

Figure 3. Calculated frequency-dependent second harmonic generation coefficients for $Ba_4AgGa_5P_8$.

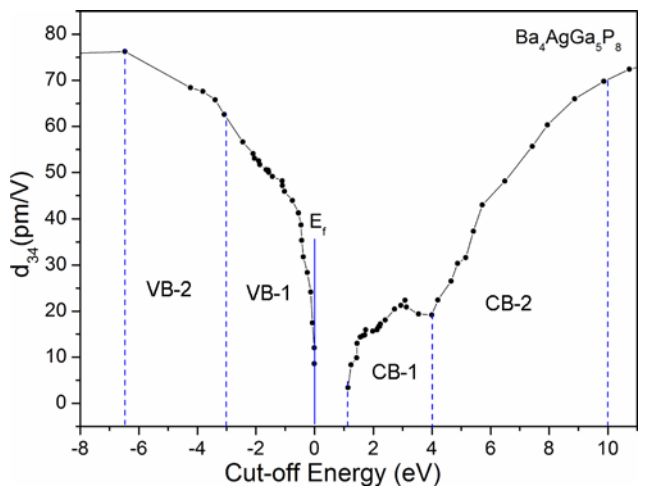

Figure 4. Cutoff-energy-depending static SHG coefficients for $Ba_4AgGa_5P_8$. The dotted line mark the different regions in VB and CB.

The origination of large SHG responses for these compounds are further analyzed based on the calculated cutoff-energy-dependent SHG coefficient (d_{34}), shown in Figure 4. From the picture it is clear that the SHG response is mostly affected by the energy bands over the ranges of VB-2 (-6.5 to -3 eV), VB-1 (-3 to 0 eV), and CB-2 (4 to 10 eV). The VB-1 and VB-2 are dominated by P 3p, Ga 4p and Ag 4d, whereas the CB-2 is contributed by P-3p, Ga-4p and Ba-5d states. Thus, the overall SHG efficiency should be mostly influenced by P-3p and Ga-4p states. So we believe that the large NLO coefficient of $Ba_4AgGa_5P_8$ arise from the distorted GaP_4 tetrahedra with a polarization parallel to the c axis.

Experimental Section

Synthesis

All manipulations were performed in an argon-filled glovebox. Starting materials were used as received: Ba (Alfa, 99%), Ga (Alfa, 99.999%), Ag (Alfa, 99.99%), Pb (Alfa, 99.99%), P (Alfa, 99.999%), As (Alfa, 99.999%). The title compounds were first synthesized from Pb-flux reactions with loading ratio of Ba:Ga:Ag:Pn:Pb = 3:1:1:5:25. The reactants were loaded in an alumina crucible and then sealed in fused silica tube under vacuum. The container was then moved to a programmable furnace, the mixture was first heated to 900 °C and homogenized at this temperature for 20 h, and then slowly cooled down to 500 °C at a rate of 5 °C/h. Finally the excessive flux was quickly decanted by centrifuge. Both compounds are stable to air and moisture. The bulk materials remain unchanged after exposed to ambient air for more than one week. Stoichiometric reactions can greatly improve the yield of the target crystals but a side product of GaPn [36] was hardly avoided in spite of various attempts. The excess Pb flux can be dissolved into the mixture of glacial acetic acid and hydrogen peroxide to improve the purity of the products. Although synthesized by using the same procedure, the crystal quality of phosphide compound is relatively poorer compared to the arsenide analogue. The refined cell parameters of $Ba_4AgGa_5P_8$ have errors of almost ten times as large as those of $Ba_4AgGa_5As_8$. However, the single crystal diffraction data of $Ba_4AgGa_5P_8$ is good for the structure solution and refinement.

Single crystal structure determination

Single crystals were selected in glovebox and cut in Paratone N oil to suitable size, and then were mounted on glass fibers for data collection. The data collections were carried on a *Bruker SMART APEX-II CCD* area detector with graphite-monochromated *Mo-Kα* radiation (λ =0.71073 Å) at 296K using *ω* scans. The frame width was 0.5° and the exposure time is 15s per frame. Data reduction and integration, together with global unit cell refinements were done by the INTEGRATE program incorporated in APEX2 software.[37] Semi-empirical absorption corrections were applied using the SCALE program for area detector.[37] The structures were solved by direct methods and refined by full matrix least-squares methods on F^2 using SHELX.[38] Both structures were refined to converge with anisotropic displacement parameters.

During the subsequent structure refinements with anisotropic thermal parameters, one 4*a* site coordinated by the Pn_4 tetrahedron exhibits very abnormal thermal parameters, which can not be solved by applying either Ga or Ag atom. Thus, refinements with this position occupied by mixed Ga and Ag were tried, which resulted in almost equal occupancies of Ga and Ag. For example, in $Ba_4AgGa_5As_8$ the freed occupancies for Ga and Ag are 50.7% and 49.3%, respectively. In addition, the other Ga site at *8c* has a freed occupancy of 99.5%. With this consideration, the problematic *4a* site was finally treated as equally occupied by Ga and Ag and the other *8c* metal site was treated as fully occupied Ga, which would turn the formula into stoichiometric and charge-balanced $Ba_4AgGa_5Pn_8$. These crystallographic results are well consistent with the analyses from Energy Dispersive X-ray Spectroscopy. In the last refinement cycles, the atomic positions for the two compounds were standardized using the program STRUCTURE TIDY.[39, 40] Crystallographic data and structural refinements are summarized in Table 1. Atomic positions and anisotropic displacement parameters are provided in Table S1. Selected bond lengths are given in Table S2. Further information in the form of CIF has been deposited with Fachinformationszentrum Karlsruhe, 76344 Eggenstein-Leopoldshafen, Germany, (fax: (49) 7247−808−666; e-mail: crysdata@fizkarlsruhe.de)−depository CSD-number 429792 and 429793 for $Ba_4AgGa_5P_8$ and $Ba_4AgGa_5As_8$, respectively.

Powder X-ray diffraction

Powder X-ray diffraction patterns were taken at room temperature by a *Bruker AXS X-ray* powder diffractometer using Cu-Kα radiation. The data were recorded in a 2*θ* mode with a step size of 0.02° and the counting time of 10 seconds. In Figure S2, the comparison between experimental and simulated data indicates the purity of the samples, which were used for subsequent measurements.

Differential Thermal Analysis and Thermogravimetry Measurements (DTA/TG)

The thermal stability was tested on the polycrystalline samples of $Ba_4AgGa_5P_8$ (mass: 37.0560 mg) and $Ba_4AgGa_5As_8$ (mass: 17.6820 mg) with a *Mettler-Toledo TGA/DSC/1600HT* instrument under the protection of high-purity argon gas. Thermogravimetric Analysis (TGA) and Differential Scanning Calorimetry (DSC) experiments were performed as well and the measured temperature range is from 300 to 1273 K with a heating rate of 10 K/min applied.

UV–Vis–NIR Diffuse Reflectance Spectrum

The optical diffuse reflectance spectra were measured using a Hitachi *U4100* spectrometer equipped with an integrating sphere attachment and $BaSO_4$ is used as a reference at room temperature. The absorption spectrum was calculated from the reflection spectrum *via* the Kubelka-Munk function: $\alpha/S = (1-R)^2/2R$, in which α is the absorption coefficient, S is the scattering coefficient, and R is the reflectance.[41]

Elemental Analysis

Energy Dispersive X-ray Spectroscopy was taken on picked single crystals of the four compounds with a Hitachi FESEM-4800 field emission microscopy equipped with a Horiba EX-450 EDS. The energy dispersive spectra (*EDS*) taken on visibly clean surfaces of the measurement proved the identical results as the crystallographic data.

Computational details

The electronic band structures, density of states (DOS) and optical properties were calculated by the Vienna Ab initio simulation package (VASP)[42-44] with the Perdew-Burke-

Ernzerh (PBE)[45] exchange-correlation functional. The projected augmented wave (PAW)[46] method with the valence states 4s and 4p for As and Ga, 4d and 5s for Ag, 5s, 5p and 6s for Ba, respectively, has been adopted. A plane-wave cutoff energy of 450 eV and a 1×3×3 *k*-point grid were used to get convergent lattice parameters throughout the geometric optimization of the lattice cell. Both the cell and atomic relaxations were carried out until the residual forces were below 0.05 eV/Å. A grid with more dense k-points of 4×12×12 was used to calculate the optical properties and DOS of the crystals. More than 350 empty bands were used in optical property calculations, and scissors operators of 0.1 eV and 0.24 eV were applied for $Ba_4AgGa_5As_8$ and $Ba_4AgGa_5P_8$, respectively.

The static and dynamic second-order nonlinear susceptibilities $\chi^{abc}(-2\omega;\omega,\omega)$ were calculated based on the length-gauge formalism derived by Aversa and Sipe[47] and modified by Rashkeev *et al.*[48] The imaginary part of static second-order optical susceptibility can be expressed as:

$$\chi^{abc} = \frac{e^3}{4\hbar^2\Omega}\sum_{nml,k}\frac{r^a_{nm}\left(r^b_{ml}r^c_{\ln}+r^c_{ml}r^b_{\ln}\right)}{2\omega_{nm}\omega_{ml}\omega_{\ln}}\left[\omega_n f_{ml}+\omega_m f_{\ln}+\omega_l f_{nm}\right]+$$

$$\frac{ie^3}{4\hbar^2\Omega}\sum_{nm,k}\frac{f_{nm}}{\omega^2_{mn}}\left[r^a_{nm}\left(r^b_{mn;c}+r^c_{mn;b}\right)+r^b_{nm}\left(r^a_{mn;c}+r^c_{mn;a}\right)+r^c_{nm}\left(r^a_{mn;b}+r^b_{mn;a}\right)\right]$$

Where r is the position operator, m, n and l are different band indices, respectively, $\hbar\omega_{nm}=\hbar\omega_n-\hbar\omega_m$ is the energy difference for the bands m and n. In order to better understand the contribution of different states to the susceptibility, the value of m and n could be tuned in our program to include some special bands. In both compounds, the equally mixed Ag and Ga2 atoms at the same sites are arranged in a checkerboard pattern in the anionic structures, which is described in details in supporting information (Figure S10).

Conclusions

In conclusion, two new quaternary pnictide-based compounds, $Ba_4AgGa_5P_8$ and $Ba_4AgGa_5As_8$, have been synthesized by the Pb-flux reactions. They are isostructural and crystallize in a noncentrosymmetric space group *Iba2* (No. 45), determined through the single-crystal X-ray diffraction techniques. The structure can be interpreted as condensed with TiNiSi-type [GaPn] slabs and (Ag,Ga)Pn_2 linear chains with Ag and Ga metals equally occupying the tetrahedral centers. Such a structural feature gives rise to a large polarization along the *c*-axis and result in strong SHG effects. The calculated cutoff-energy-dependent SHG coefficients are 77.4 pm/V and 107.1 pm/V for $Ba_4AgGa_5P_8$ and $Ba_4AgGa_5As_8$, respectively, which are about two times larger than the d_{36} of $AgGaSe_2$. In addition, the birefringence (Δn) is moderate for both compounds as well, 0.157 and 0.206 for $Ba_4AgGa_5P_8$ and $Ba_4AgGa_5As_8$, implying that the two crystals may be suitable for the phase-matching condition in the SHG process.

Acknowledgements

The authors acknowledge the financial support from the National Natural Science Foundation of China (Grant Nos. 51271098, 51321091).

Notes and references

[a] State Key Laboratory of Crystal Materials, Institute of Crystal Materials, Shandong University, Jinan, Shandong 250100, People's Republic of China.

[b] Fujian Institute of Research on the Structure of Matter, Chinese Academy of Sciences, Fuzhou, Fujian, 350002, People's Republic of China.

Email: shqxia@sdu.edu.cn; wkc@fjirsm.ac.cn

†Electronic Supplementary Information (ESI) available: The X-ray crystallographic file in CIF format of the title compounds; positional and equivalent isotropic displacement parameters and selected bond distances of two compounds; TG-DSC data of the polycrystalline samples of both compounds; powder X-ray diffraction patterns of the polycrystalline samples of the title compounds; the optical absorption spectrum measured on polycrystalline samples; the calculated electronic structures and optical properties of both compounds; coordination geometry plot for Ba cations in $Ba_4AgGa_5P_8$; the structure model of $Ba_4AgGa_5Pn_8$ for electronic structure calculations; Ball and stick structure view of $Ba_4AgGa_5P_8$, viewed down the c-axis; EDX analysis on the composition of a single crystals for $Ba_4AgGa_5P_8$ and $Ba_4AgGa_5As_8$. See DOI: 10.1039/b000000x/

1 C. T. Chen, Y. C. Wu, A. D. Jiang, B. C. Wu, G. M. You, R. K. Li and S. J. Lin, *J. Opt. Soc. Am. B*, 1989, **6**, 616.

2 Y. C. Wu, T. Sasaki, S. Nakai, A. Yokotani, H. G. Tang and C. T. Chen, *Appl. Phys. Lett.*, 1993, **62**, 2614.

3 C. F. Sun, C. L. Hu, X. Xu, J. B. Ling, T. Hu, F. Kong, X. F. Long and J. G. Mao, *J. Am. Chem. Soc.*, 2009, **131**, 9486.

4 H. S. Ra, K. M. Ok, P. S., Halasyamani, *J. Am. Chem. Soc.*, 2003, **125**, 7764.

5 C. T. Chen, B. C. Wu, A. D. Jiang and G. M. You, *Sci. Sin., Ser. B*, 1985, **28**, 235.

6 R. C. Eckardt, H. Masuda, Y. X. Fan and R. L. Byer, *IEEE J. Quantum Electon.*, 1990, **26**, 922.

7 A. Harasaki and K. Kato, *Jpn. J. Appl. Phys.*, 1997, **36**, 700.

8 P. Canareli, Z. Benko, A. H. Hielscher, R. F. Curl and F. K. Tittel, *IEEE J. Quantum Electon.*, 1992, **28**, 52.

9 B. Tell and H. M. Kasper, *Phys. Rev. B.*, 1971, **4**, 4455.

10 R. L. Byer, M. M. Choy, R. L. Herbst, D. S. Chemla and R. S. Feigelson, *Appl. Phys. Lett.*, 1974, **24**, 65.

11 G. D. Boyd, E. Buehler and F. G. A. Storz, *Appl. Phys. Lett.*, 1971, **18**, 301.

12 G. D. Boyd, T. J. Bridges and C. K. N. Patel, *Appl. Phys. Lett.*, 1972, **21**, 553.

13 G. A. Verozubova, A. O. Okunev, A. I. Gribenyukov, A. Yu. Trofimiv, E. M. Trukhanov and A. V. Kolesnikov, *J. Cryst. Growth*, 2010, **312**, 1122.

14 M. J. Zhang, B. X. Li, B. W. Liu, Y. H. Fan, X. G. Li, H. Y. Zhang and G. C. Guo, *Dalton Trans.*, 2013, **42**, 14223.

15 K. Feng, L. Kang, Z. S. Lin, J. Y. Yao and Y. C. Wu, *J. Mater. Chem. C*, 2014, **2**, 4590.

16 X. S. Li, L. Kang, C. Li, Z. S. Lin, J. Y. Yao and Y. C. Wu, *J. Mater. Chem. C*, 2015, **3**, 4754.

17 M. J. Zhang, X. M. Jiang, L. J. Zhou and G. C. Guo, *J. Mater. Chem. C*, 2013, **1**, 3060.

18 T. K. Bera, J. I. Jang, J. B. Ketterson and M. G. Kanatzidis, *J. Am. Chem. Soc.*, 2009, **131**, 75.
19 M. C. Chen, L. M. Wu, H. Lin, L. J. Zhou and L. Chen, *J. Am. Chem. Soc.*, 2010, **134**, 6058.
20 S. M. Kuo, Y. M. Chang, I. Chung, J. I. Jang, B. H. Her, S. H. Yang, J. B. Ketterson, M. G. Kanatzidis and K. F. Hsu, *Chem. Mater.*, 2013, **25**, 2427.
21 E. Lallier, M. Brevignon and J. Lehoux, *Opt. Lett.*, 1998, **23**, 1511.
22 L. A. Eyres, P. J. Tourreau, T. J. Pinguet, C. B. Ebert, J. S. Harris, M. M. Fejer, L. Becouarn, B. Gerard and E. Lallier, *Appl. Phys. Lett.*, 2001, **79**, 904.
23 W. R. L. Lambrecht and X. S. Jiang, *Phys. Rev. B.*, 2004, **70**, 045204.
24 R. L. Byer, H. Kildal and R. S. Feigelson, *Appl. Phys. Lett.*, 1971, **19**, 237.
25 X. C. Liu, N. Lin, J. Wang, M. Y. Pan, X. Zhao, X. T. Tao and S. Q. Xia, *Inorg. Chem.*, 2013, **52**, 11836.
26 C. B. Shoemaker and D. P. Shoemaker, *Acta Cryst.*, 1965, **18**, 900.
27 B. Saparov and S. Bobev, *Inorg. Chem.*, 2010, **49**, 5173.
28 K. Peters, W. Carrillo Cabrera, M. Somer and H. G. von Schnering, *Z. Kristallogr.*, 1996, **211**, 53.
29 A. M. Goforth, H. Hope, C. L. Condron, S. M. Kauzlarich, N. Jensen, P. Klavins, S. MaQuilon and Z. Fisk, *Chem. Mater.*, 2009, **21**, 4480.
30 A. Mewis, *Z. Naturforsch., Teil B: Anorg. Chem.*, 1979, **34**, 1373.
31 Z. J. Ma, K. C. Wu, R. J. Sa, Q. H. Li and Y. F. Zhang, *J. Alloy Compd.*, 2013, **586**, 16.
32 G. H. Zou, Z. J. Ma, K. C. Wu and N. Ye, *J. Mater. Chem.*, 2012, **22**, 19911.
33 Y. Z. Huang, L. M. Wu, X. T. Wu, L. H. Li, L. Chen and Y. F. Zhang, *J. Am. Chem. Soc.*, 2010, **132**, 12788.
34 D. A. Kleinman, *Phys. Rev.*, 1962, **126**, 1977.
35 V. G. Dmitriev, G. G. Gurzadyan and D. N. Nikogosyan, H*andbook of Nonlinear Optical Crystals*, Springer, Berlin, 1999.
36 A. Addamiano, *J. Am. Chem. Soc.*, 1960, **82**, 1537.
37 Bruker APEX2; Bruker AXS Inc.: Madison, WI, 2005.
38 G. M. Sheldrick, *SHELXTL*, University of Göttingen, Göttingen, Germany, 2001.
39 E. Parthé and L. M. Gelato, *Acta Crystallogr.*, 1984, **40**, 169.
40 L. M. Gelato and E. Parthé, *J. Appl. Crystallogr.*, 1987, **20**, 139.
41 G. Kortüm and J. E. Lohr, *Reflectance Spectroscopy: principles, methods, applications*, Springer-Verlag: New York, 1969.
42 G. Kresse, Vienna ab initio simulation package (VASP).
43 G. Kresse and J. Furthmuller, *Phys. Rev. B: Condens Matter*, 1996, **54**, 11169.
44 G. Kresse and D. Joubert, *Phys. Rev. B: Condens Matter*, 1999, **59**, 1758.
45 J. P. Perdew, K. Burke and M. Ernzerhof , *Phys. Rev. Lett.*, 1996, **77**, 3865.
46 P. E. Blochl, *Phys. Rev. B: Condens Matter*, 1994, **50**, 17953.
47 C. Aversa and J. E. Sipe, *Phys. Rev. B*, 1995, **52**, 14636.
48 S. N. Rashkeev, W. R. L. Lambrecht and B. Segall, *Phys. Rev. B*, 1998, **57**, 3905.

Table of Contents Graphic artwork

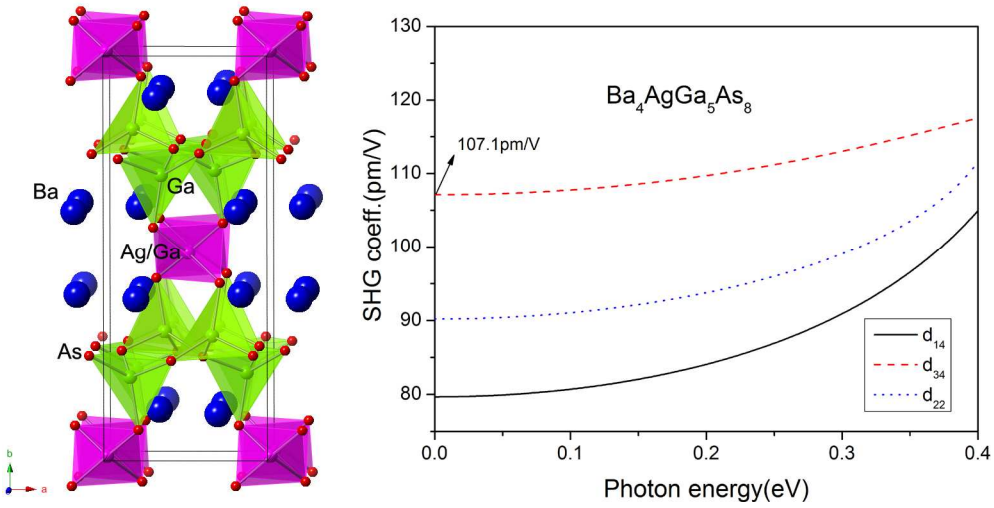

Synopsis

Two new quaternary pnictide-based compounds with noncentrosymmetric space group *Iba2* (No. 45), $Ba_4AgGa_5P_8$ and $Ba_4AgGa_5As_8$, were synthesized through the Pb-flux reactions. Their structure feature TiNiSi-type [GaPn] slabs and $(Ag,Ga)Pn_2$ linear chains with Ag and Ga atoms equally occupying the tetrahedral centers, which results in large polarization along the *c*-axis and strong SHG response. The calculated cutoff-energy-dependent SHG coefficients are 77.4 pm/V and 107.1 pm/V for $Ba_4AgGa_5P_8$ and $Ba_4AgGa_5As_8$, respectively, which are about two times larger than the d_{36} of $AgGaSe_2$.